Survey of Ring Current Composition During Magnetic Storms

DTIC QUALITY INSPECTED 4

15 February 1998

Prepared by

M. GRANDE and C. H. PERRY
Rutherford Appleton Lab, Chilton, UK

A. HALL
University of Leicester, UK

J. FENNELL
The Aerospace Corporation, Los Angeles, CA

B. WILKEN
Max Planck Institute fur Aeronomie, Germany

Prepared for

SPACE AND MISSILE SYSTEMS CENTER
AIR FORCE MATERIEL COMMAND
2430 E. El Segundo Boulevard
Los Angeles Air Force Base, CA 90245

Engineering and Technology Group

19980415 148

THE AEROSPACE CORPORATION
El Segundo, California

This report was submitted by The Aerospace Corporation, El Segundo, CA 90245-4691, under Contract No. F04701-93-C-0094 with the Space and Missile Systems Center, 2430 E. El Segundo Blvd., Los Angeles Air Force Base, CA 90245. It was reviewed and approved for The Aerospace Corporation by A. B. Christensen, Principal Director, Space and Environment Technology Center. Col. C. Whited was the project officer for the Mission-Oriented Investigation and Experimentation (MOIE) program.

This report has been reviewed by the Public Affairs Office (PAS) and is releasable to the National Technical Information Service (NTIS). At NTIS, it will be available to the general public, including foreign nationals.

This technical report has been reviewed and is approved for publication. Publication of this report does not constitute Air Force approval of the report's findings or conclusions. It is published only for the exchange and stimulation of ideas.

C. WHITED, COL, USAF

SMC/SDE AXES

J. W. COLE, MAJ, USAF

REPORT DOCUMENTATION PAGE

Public reporting burden for this collection of information is estimated to average 1 hour per response, including the time for reviewing instructions, searching existing data sources, gathering and maintaining the data needed, and completing and reviewing the collection of information. Send comments regarding this burden estimate or any other aspect of this collection of information, including suggestions for reducing this burden to Washington Headquarters Services, Directorate for Information Operations and Reports, 1215 Jefferson Davis Highway, Suite 1204, Arlington, VA 22202-4302, and to the Office of Management and Budget, Paperwork Reduction Project (0704-0188), Washington, DC 20503.

1. AGENCY USE ONLY (*Leave blank*)	2. REPORT DATE 15 February 1998	3. REPORT TYPE AND DATES COVERED

4. TITLE AND SUBTITLE

Survey of Ring Current Composition During Magnetic Storms

5. FUNDING NUMBERS

F04701-93-C-0094

6. AUTHOR(S)

M. Grande, C. H. Perry, A. Hall, J. Fennell, and B. Wilken

7. PERFORMING ORGANIZATION NAME(S) AND ADDRESS(ES)

The Aerospace Corporation
Technology Operations
El Segundo, CA 90245-4691

8. PERFORMING ORGANIZATION REPORT NUMBER

TR-98(8570)-3

9. SPONSORING/MONITORING AGENCY NAME(S) AND ADDRESS(ES)

Space and Missile Systems Center
Air Force Materiel Command
2430 E. El Segundo Boulevard
Los Angeles Air Force Base, CA 90245

10. SPONSORING/MONITORING AGENCY REPORT NUMBER

SMC-TR-98-08

11. SUPPLEMENTARY NOTES

12a. DISTRIBUTION/AVAILABILITY STATEMENT

Approved for public release; distribution unlimited

12b. DISTRIBUTION CODE

13. ABSTRACT (*Maximum 200 words*)

During geomagnetic storms, the ring current is substantially modified and intensified. We use data from the MICS instrument on CRRES to investigate composition changes in magnetospheric ions in the energy range 20–400 keV/e. These are related to the Dst signature of the storm. Long-term survey plots of MICS data show that during storms there is an initial increase of ionospheric material at around $L = 3$. The peak in the ratio of ionospheric material rises to higher L-shells during the storm recovery. By contrast, solar wind material remains predominantly at higher L-shells, and a belt of ring current alpha particles forms around $L = 4$. The L-shell of the peak fraction of ionospheric material is a strong function of Dst. Substorm composition reflects the background composition at that L-shell. These results are emphasized by a superposed epoch analysis of substorm injection composition. It shows that the composition of storm time injections is similar to a set of oxygen-rich injections. We conclude that, during the solar maximum interval that CRRES observed, substorms are not directly responsible for the ring current oxygen population.

14. SUBJECT TERMS

Ring current, CRRES, Ion composition, Energetic particles

15. NUMBER OF PAGES

6

16. PRICE CODE

17. SECURITY CLASSIFICATION OF REPORT	18. SECURITY CLASSIFICATION OF THIS PAGE	19. SECURITY CLASSIFICATION OF ABSTRACT	20. LIMITATION OF ABSTRACT
UNCLASSIFIED	UNCLASSIFIED	UNCLASSIFIED	

NSN 7540-01-280-5500

Standard Form 298 (Rev. 2-89)
Prescribed by ANSI Std. Z39-18
298-102

Acknowledgments

Contents

Figures

Table

1 INTRODUCTION

The CRRES spacecraft was launched into a geostationary transfer orbit on 25th July 1990. The 13 month mission thus took place near Solar Maximum, and a number of major Dst excursions were observed during this time. The eccentric nature of the orbit and the inclination of 18.1 degrees meant that CRRES sampled a range of L-shells up to L=8 and magnetic latitudes within 30 degrees of the magnetic equator. The MLT of apogee ranged from about 08:30 after launch to about 15:30 by the end of the mission. This spatial coverage of the magnetosphere has proved extremely useful, enabling the effect of position of observation on substorm particle injection signature to be investigated. It also enables us to survey the magnetospheric ion population throughout the mission, with a data set large enough to permit meaningful statistical conclusions.

The details of the MICS sensor have been discussed elsewhere (Wilken et al, 1991). An ion intercepted by the spectrometer first passes through a collimator and an electrostatic analyser. For a specific voltage applied to the analyser, only ions of a particular energy per charge can traverse the full length. The applied voltage is varied in 32 logarithmic steps, each of 0.256 sec duration. Each step determines an energy per unit charge (E/Q) band within the overall range 1 to 425 keV/e, for which ions pass through the analyser and are then post-accelerated into the time-of-flight (TOF) unit, before finally undergoing a total energy (E) dump in the solid state detector. These three measurements E, TOF and E/Q can be combined on board to extract the energy, charge (Q) and mass (M) of the ion. An integrated table of the assigned M vs. M/Q bin is accumulated every 8 energy sweeps. It contains species counts, integrated over the energy range from 30-425 keV/e, with no trigger mode bias. It is subject to slight blurring at the lower energy cut-off, due to variable threshold effects for different species, but analysis shows that this does not alter the results presented here.

2 ANALYSIS & RESULTS

Using the unbiased data set from the M vs. M/Q table we produced a survey of the ring current during the second half of the CRRES mission, a highly disturbed period. We have taken all data from the period between orbits 417 and 1067, corresponding to days 13 to 283 of 1991. Due to the orbital geometry this was also the period during which the majority of substorm dispersionless injections were observed. Each orbit comprises an outbound and an inbound leg which are ordered according to time and then averaged by L-shell. The panels on the left of Figure 1 show the long term temporal evolution of ring current material, respectively singly charged helium (He^+), alpha particles (He^{++}), singly charged oxygen (O^+) and the composition ratios He^+/He^{++} and O^+/He^{++}.

During a storm, the peak number density of the ionospheric material, represented by O^+, shown in Figure 1, panel 3, is initially at a low (<3.5) L shell; the higher the Dst the lower the L of the peak. This peak rises as the storm decays, suggesting transport of ionospheric material to higher L-shell, or preferential loss at lower L. By contrast, the peak in the number density of alpha particles (Figure 1, panel 2), which should be characteristic of solar wind material, appears to split during recovery from a storm, and to produce a belt centred on L=3 to 3.5, which persists on a time scale of weeks. It has a characteristic energy of 0.5 to 1 MeV, and is strongly 90° pitch angle aligned. In addition, a component persists at high L, while in the region between L=4 and 5 there is a dip. Detailed comparison of the He^+ (Figure 1, panel 1) and He^{++} (Figure 1, panel 2) plots shows that as the storm decays, this dip in He^{++} grows. However, it does not, in general, correspond to the quiet time maximum in the He^+ number density at L=4.5. This is not compatible with the suggestion that the solar origin He^{++} is decaying in this region via charge exchange, and is thus responsible for the majority of the post storm He^+ population. Only in the quietest periods with Dst above -20 nT do we consider this process, as described by Fritz and Spelvijk (1978) and Grande et. al. (1993) to be dominant. The CNO high charge group (not shown) does not show the belt at low energy exhibited for He^{++}. This is presumably due to a higher charge exchange cross section, or a stronger coupling to another loss process.
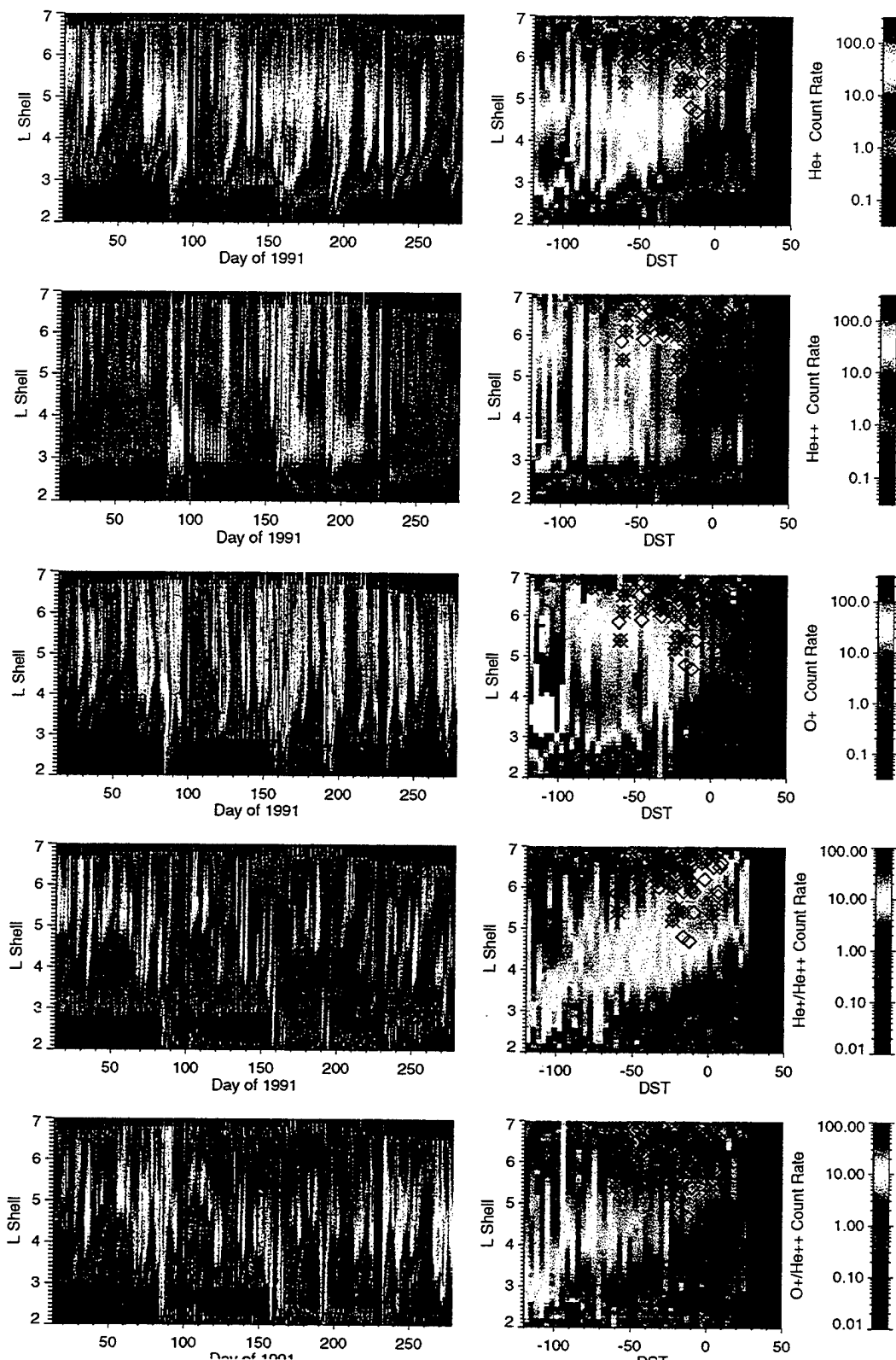
Fig 1. Behaviour of ring current ions with L-Shell as a function of day number (left-hand panels) and DST (right hand panels). Count rates for He+, He++ and O+ are shown in the top three sets of panels and the ratio of count rates for, He+/He++ and O+/He++ in the bottom two sets
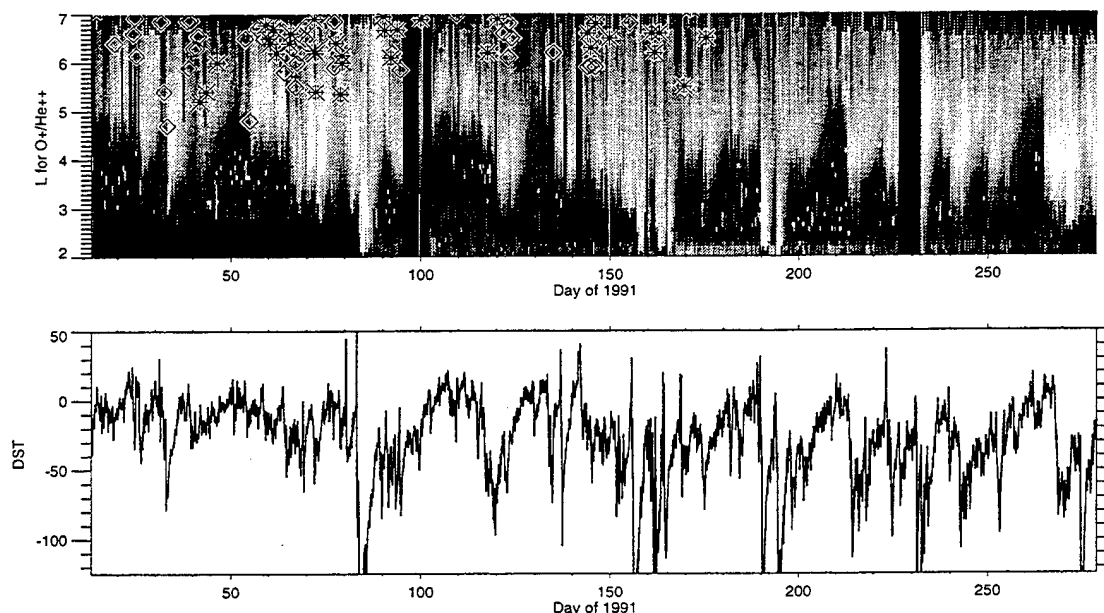
Fig 2   *Upper Panel* The Ratio O^+/He^{++} is plotted as grey scale, as a function of L shell vs. day number .Position of Substorms are superimposed. *Lower Panel* shows Dst on the same time scale to show the correspondence.

While the correlation with Dst is striking, it is necessary to quantify it. For each orbit, we have derived the mean L-shell for a given species, by weighting with the count rates, which correspond to differential energy flux. In Figure 3 we plot the derived value of mean L-shell against Dst, for H, He^+, He^{++}, O^+, and the ratios He^+/He^{++} and O^+/He^{++}. Although these ratios might vary systematically due to the different energy thresholds of different species, and the tendency for radial diffusion to increase energies at lower L, our analysis suggests that in practice this effect is not significant. It is seen that there is a strong correlation with Dst for O^+ and He^+, the species generally considered to be ionospheric. There is a weak anticorrelation for He^{++}. A surprising feature is that although the proton data here is not directly comparable to the heavier species, since there is an instrumental mode change for protons only at L=4, above this value the mean L-shell of protons in our energy range is almost independent of Dst. The regression line is overplotted. We also divided the plot between Dst greater and less than -30, indicating storm and non-storm periods, and calculated the regression lines for each condition. Except in the case of He^{++}, there was no obvious difference in the trend for each half. There is a break in the trend for He^{++}, which corresponds to a slight change in the opposite sense for He^+ which may be indicative of the occurrence of the charge exchange process in quiet times.

In the right hand panels of Figure 1 we have reordered the data in the left hand panels, plotting it against Dst. Each vertical cut therefore shows the average differential flux for that species for a given Dst. Horizontal cuts show the change in this flux with Dst at a given L-shell for a given species. Several trends are particularly noticeable. For singly charged Helium we see that the peak composition varies smoothly from around L= 5.3 at low Dst to L=3.4 at high Dst. A very similar behaviour is seen for singly charged oxygen. It should be emphasised that these measurements were made near solar maximum. Observations by the recently launched Polar satellite, during a solar minimum period show very little oxygen, and different mechanisms may be at work. It may be that at solar minimum substorm activity is more important for producing ionospheric outflow.

Plotting the ratio of He^+/He^{++} (Figure 1 panel 4), we find a continuous peak in the ratio, which moves up and down in L-shell; the L-shell of this peak shows a strong correlation with Dst, with low altitude corresponding to a large negative Dst excursion. The bottom row shows O^+/He^{++}. While the He^{++} is certainly likely to be of solar origin, the provenance of the He^+ is less certain. It is probably mostly ionospheric material, with some contribution from ions derived from high L-shell He^{++} which have radially diffused to lower L shells, and undergone trapping and charge
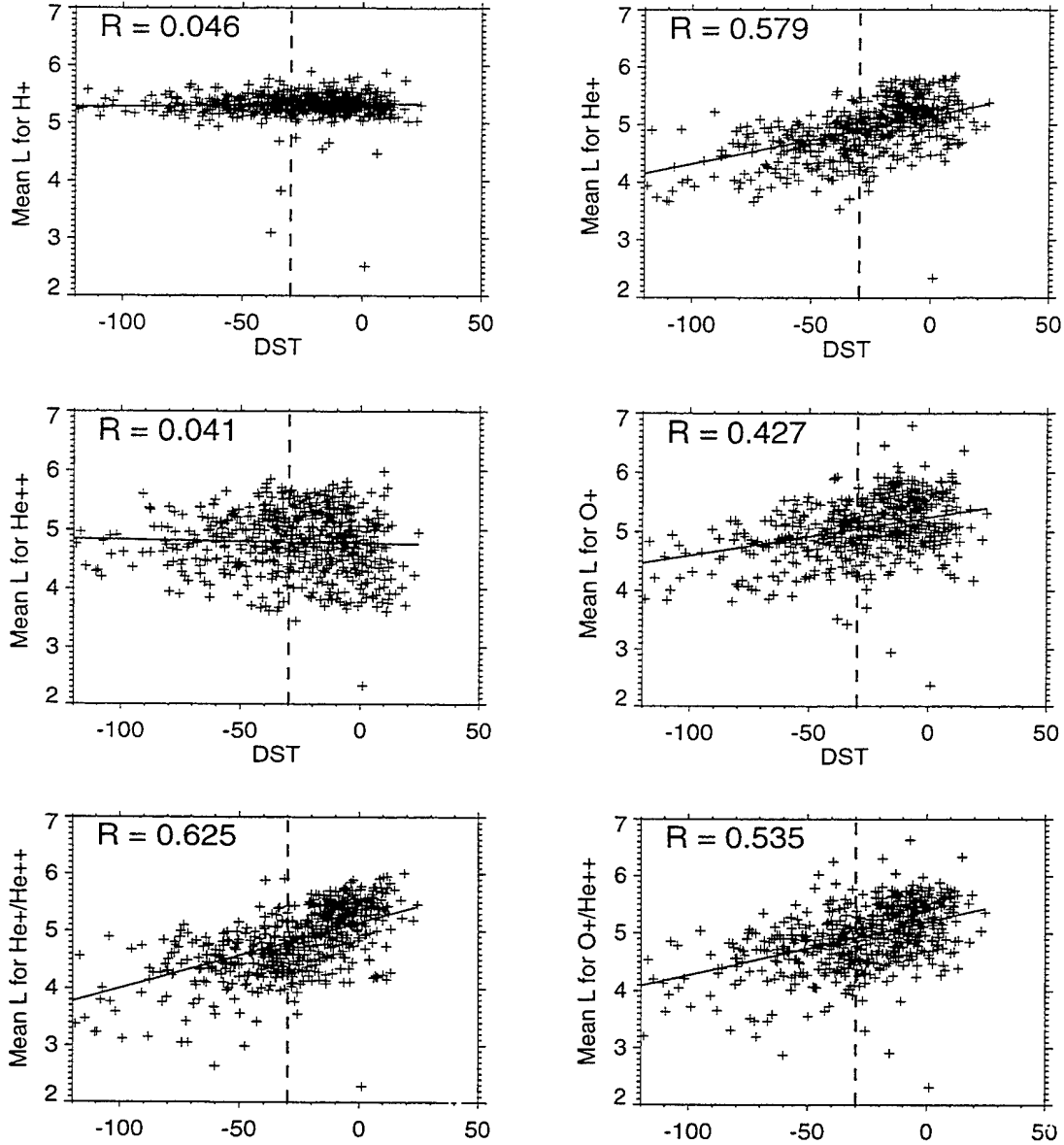
3

Fig 3   L-shell of composition peak plotted against Dst, for H, He+, He++, O+, and the ratios He+/He++, O+/He++. The Regression line is overplotted., to show the L dependence of each species or ratio peak on Dst .

exchange, as discussed above. There seems to be more evidence from the survey for the ionospheric process, in that the L-shell distribution of He^+ follows that of O^+. Excesses of He^+ relative to O^+ occur in quiet times, but do not show a strong relation to He^{++} distribution. The ratio of He^+ to O^+ (not plotted) is essentially flat, except for a slight excess of O^+ at high L, suggesting that the processes are linked.

In Figure 1 (right hand panels) we have superimposed the 87 events which form the database of dispersionless substorm energetic particle injections observed by CRRES, and which will be the basis of the investigation of differences in storm and quiet time events in the next section. In general He^+ is not present in injections, while O^+ is. It therefore follows that the process which produces the similar distributions of these two ionospheric components cannot be direct substorm energisation. The injections themselves are observed at higher L-shells than the peak in the ratio of ionospheric to solar-wind material. A cross correlation of the derived mean L for the ratio of He^+/He^{++} with Dst shows that on the timescale of the averaging, namely one ten hour orbit, there is no lag, indicating a prompt dependence on Dst. It will be a fruitful area for future work to investigate this relationship on finer timescales. In the following section we discuss changes in the composition ratio on timescales associated with substorms.

4

3 SUPERPOSED EPOCH ANALYSIS

Using the same set of dispersionless injection events as Hall et al, a superposed epoch analysis was conducted. The data set was subdivided in order to investigate the behaviour of the different ion species and different magnetospheric activity regimes as defined by the Dst index. Again, we use Dst ≤ -30 nT to characterise storm time and Dst > -30 nT to characterise non-storm time. Events were aligned using the onset time, with integrated count rates above 70 keV/e calculated for one hour on either side. For each time step the mean was determined from the distribution of all events at that time. Due to the inclusion of "multiple" type injection events in both subsets, we examine only the behaviour of the first onset.

	Storm-time		Quiet-time	
	1 hr	*onset*	*1 hr*	*onset*
H^+	100	80	60	80
He^+	6	3.5	3	2.5
He^{++}	10	9	2.5	4.5
O^+	8	4	1	1.5
$H^+:He^+$	20:1	22:1	17:1	20:1
$H^+:He^{++}$	10:1	8:1	23:1	17:1
$H^+:O^+$	14:1	18:1	50:1	40:1

Table 1: Storm and quiet time composition comparisons one hour before and immediately prior to onset for ion species and their ratios

First we consider the behaviour before onset. The details are shown in Table 1, where in each case the first figure represents the count rate one hour prior to onset, and the second that just prior to onset. Note also that the background levels for each species are much higher before onset during storms, as expected. The singly charged oxygen count rate shows the largest difference in agreement with Daglis el. al. (1996). For storms, there is a drop in the count rate during the hour before onset. The quiet time ratio of H^+/He^{++} (20:1) is numerically very similar to that expected in the solar wind, however, the storm time value appears to have been enriched with He^{++} by a factor 2. Interestingly the only ratio which is roughly unchanged is H^+/He^+.

The comparison of superposed analyses of 37 storm events and 50 non-storm time events behaviour of individual ion species is shown in Fig 4. One immediately obvious feature is that whereas the non-storm events are peaks in ion count rate (Figure 4a) the storm time injections correspond to steps(Figure 4b). The trend is slightly more pronounced for He^{++}. This is probably due to the likelihood of subsequent injections during a storm period; the average of these produces the step. As remarked above, we see that the backgrounds are higher before onset during storm time. There is no difference between O^+ and He^{++} magnitudes in either storm or non-storm. Multiple injections do not show an average oxygen increase, although this can be seen in several individual cases. In both cases the

effect on He$^+$ is marginal. In Figure 5 we show the result of a superposed analysis of the ratio of O$^+$ to He^{++}. This ratio remains unchanged during quiet time, but changes by a factor 2 during storm time. However, the largest change occurs in a subset labelled O$^+$ rich, which comprises only 10 events. They are selected as the events which show the largest percentage increase in O$^+$ at onset in the statistical survey. It is seen that they are characterised by a large O$^+$ background prior to onset, and a large drop in the preceding hour. Of these 10 events only 4 have a Dst less than -30. In other words, the majority are non-storm events. We conclude that the behaviour in storms is like events having a high oxygen background and of course this is the case in storms. This suggests that it is the likelihood of a high background proportion of O$^+$ which leads to the increase in O$^+$/He^{++} ratio increase at substorm onset during a storm.

4 CONCLUSIONS

The ratio of ionospheric to solar wind material in the ring current shows a peak in L-shell, whose value correlates with negative excursions in Dst. Substorms generally take place at higher L-shells than this peak. Although there is a tendency for an O$^+$/He^{++} ratio increase to occur during a stormtime substorm, the average behaviour is strongly influenced by a few events having a high initial O$^+$ concentration, and high initial oxygen substorms show this increase in non-storm times also. That the O$^+$ concentration in the ring current increases during storms is well known. Here we have argued that the reason for this cannot however be attributed directly to substorm associated processes.

Fig 4 Superposed Epoch analysis of 87 substorms, showing the timeline of individual species in non-storm times (*above*) and storm times(*below*)

Fig 5 Superposed epoch analysis showing evolution of the ratio of O$^+$/He^{++} ions for O$^+$ rich, multiple onset, stormtime and non-stormtime substorms.

References

Daglis I. A., W. I. Axford, S. Livi, B. Wilken, M. Grande, F. Soraas, Auroral Ionospheric Ion Feeding of the Inner Plasma Sheet during Substorms. *J Geomag. Geoelec.*, **48** 729-740, (1996).

Fritz T. A. and W Spelvijk, Energetic ionised He in the quiet time radiation belts, *J. Geophys. Res.*, **83**, 654-662 (1978).

Hall A & al, Survey of Dispersionless Substorm Ion Injections Observed by CRRES, (*this proceedings*).

Grande M., C.H.Perry, D.R.Lepine, D.S. Hall, D.A.Bryant, J.F.Fennell, B.Wilken, T.A. Fritz, Solar Wind Alpha Particles as a Source of Magnetospheric Helium. AGU Fall Meeting SM12A-7 (1993).

Wilken, B., W. Weiss, D. Hall, M. Grande, F. Soraas, and J. F. Fennell, The magnetospheric ion composition spectrometer MICS onboard CRRES, *J. Spacecraft and Rockets*, **29**, 585-591. (1992).
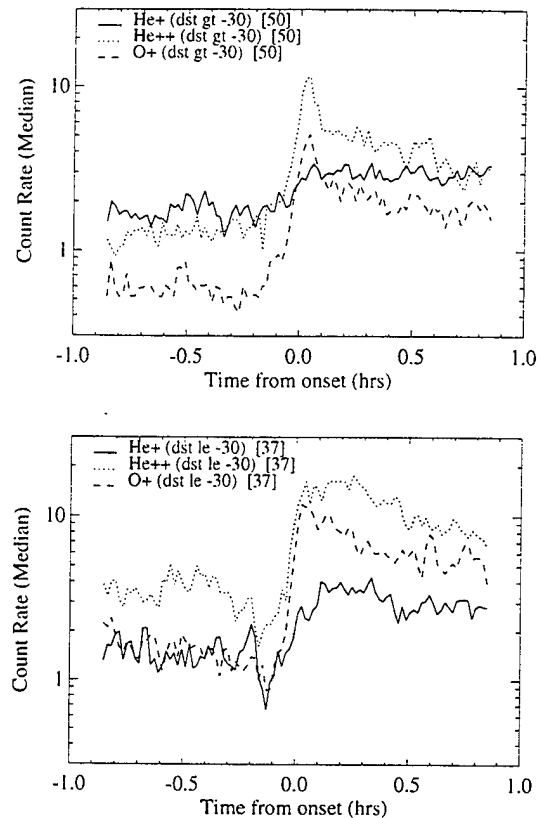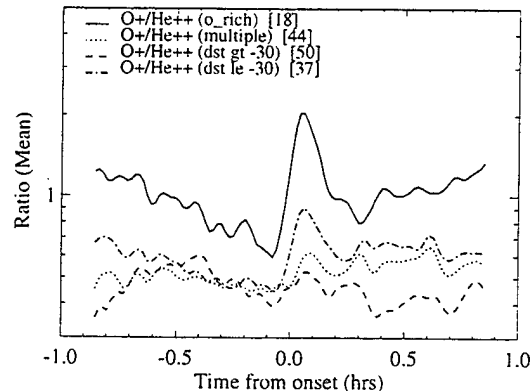
TECHNOLOGY OPERATIONS

The Aerospace Corporation functions as an "architect-engineer" for national security programs, specializing in advanced military space systems. The Corporation's Technology Operations supports the effective and timely development and operation of national security systems through scientific research and the application of advanced technology. Vital to the success of the Corporation is the technical staff's wide-ranging expertise and its ability to stay abreast of new technological developments and program support issues associated with rapidly evolving space systems. Contributing capabilities are provided by these individual Technology Centers:

Electronics Technology Center: Microelectronics, VLSI reliability, failure analysis, solid-state device physics, compound semiconductors, radiation effects, infrared and CCD detector devices, Micro-Electro-Mechanical Systems (MEMS), and data storage and display technologies; lasers and electro-optics, solid state laser design, micro-optics, optical communications, and fiber optic sensors; atomic frequency standards, applied laser spectroscopy, laser chemistry, atmospheric propagation and beam control, LIDAR/LADAR remote sensing; solar cell and array testing and evaluation, battery electrochemistry, battery testing and evaluation.

Mechanics and Materials Technology Center: Evaluation and characterization of new materials: metals, alloys, ceramics, polymers and composites; development and analysis of advanced materials processing and deposition techniques; nondestructive evaluation, component failure analysis and reliability; fracture mechanics and stress corrosion; analysis and evaluation of materials at cryogenic and elevated temperatures; launch vehicle fluid mechanics, heat transfer and flight dynamics; aerothermodynamics; chemical and electric propulsion; environmental chemistry; combustion processes; spacecraft structural mechanics, space environment effects on materials, hardening and vulnerability assessment; contamination, thermal and structural control; lubrication and surface phenomena; microengineering technology and microinstrument development.

Space and Environment Technology Center: Magnetospheric, auroral and cosmic ray physics, wave-particle interactions, magnetospheric plasma waves; atmospheric and ionospheric physics, density and composition of the upper atmosphere, remote sensing, hyperspectral imagery; solar physics, infrared astronomy, infrared signature analysis; effects of solar activity, magnetic storms and nuclear explosions on the earth's atmosphere, ionosphere and magnetosphere; effects of electromagnetic and particulate radiations on space systems; component testing, space instrumentation; environmental monitoring, trace detection; atmospheric chemical reactions, atmospheric optics, light scattering, state-specific chemical reactions and radiative signatures of missile plumes, and sensor out-of-field-of-view rejection.